

Tribological performance at high temperatures of alumina coatings applied by plasma spraying process onto a refractory material

D. Franco, E. López, F. Vargas, Hélène Ageorges

▶ **To cite this version:**

D. Franco, E. López, F. Vargas, Hélène Ageorges. Tribological performance at high temperatures of alumina coatings applied by plasma spraying process onto a refractory material. Surface and Coatings Technology, 2019, 371, pp.276-286. 10.1016/j.surfcoat.2019.04.058 . hal-02188060

HAL Id: hal-02188060

https://unilim.hal.science/hal-02188060

Submitted on 25 Oct 2021

HAL is a multi-disciplinary open access archive for the deposit and dissemination of scientific research documents, whether they are published or not. The documents may come from teaching and research institutions in France or abroad, or from public or private research centers.

L'archive ouverte pluridisciplinaire **HAL**, est destinée au dépôt et à la diffusion de documents scientifiques de niveau recherche, publiés ou non, émanant des établissements d'enseignement et de recherche français ou étrangers, des laboratoires publics ou privés.



Distributed under a Creative Commons Attribution - NonCommercial 4.0 International License

Version of Record: https://www.sciencedirect.com/science/article/pii/S0257897219304293
Manuscript_3d43188967d9e7114c8cdc2a38f9cae1

TRIBOLOGICAL PERFORMANCE AT HIGH TEMPERATURES OF ALUMINA COATINGS APPLIED BY PLASMA SPRAYING PROCESS ONTO A REFRACTORY MATERIAL

D. Franco [a, b, *], H. Ageorges [a], E. López [b] and F. Vargas [b]

[a] University of Limoges (Limoges – France). ECNRS, IRCER, UMR7315, F-87000.

[b] University of Antioquia (Medellín – Colombia), GIPIMME-GIMACYR Research Groups.

[*] Corresponding author: idavid.franco@udea.edu.co

Abstract

Two different Al_2O_3 coatings manufactured by plasma spraying process were tested under dry sliding contact conditions at high temperatures in order to determine their tribological behavior. At higher temperature than 800 °C, wear rate and mechanisms for Al_2O_3 coatings have not yet been reported. The results obtained were compared with those from both: an electro-melted Al_2O_3 refractory used as reference and a pressed & sintered silico-aluminous refractory used as substrate, which were tested under the same conditions. The reference was chosen due to the high performance against wear that this material shows, and the substrate was chosen due to the high potential that this material with low properties against wear shows when it is coated. Crystallographic phases, micro-hardness, Young's modulus

© 2019 published by Elsevier. This manuscript is made available under the CC BY NC user license
https://creativecommons.org/licenses/by-nc/4.0/

and fracture toughness were measured before and after the wear tests, obtaining as results that both Al_2O_3 coatings showed better wear performance than the pressed & sintered silico-aluminous refractory used as substrate, and even than the electro-melted Al_2O_3 refractory used as reference. Additionally, in the plasma sprayed coatings, as well as, in the electro-melted Al_2O_3 refractory, the wear mechanism was controlled by a transformation produced by the increasing in temperature from ductile deformation to brittle deformation, for finally returning to ductile deformation again. The high performance of plasma sprayed coatings was mainly due to the high values of toughness, as well as due to the increasing of the α-Al_2O_3 levels and therefore, the hardness during the wear tests because of the high temperature, allowing to these ceramic coatings to be a possible way to protect the conventional pressed & sintered silico-aluminous refractories to replace the expensive non-structural electro-melted ones currently exposed to abrasive wear in glass, cement and other primary industries.

Keywords

Plasma sprayed Al_2O_3 coatings, Electro-melted Al_2O_3 refractory, Pressed & sintered silico-aluminous refractory, Sliding contact, Tribology at high temperature.

1. INTRODUCTION

Atmospheric Plasma Sprayed (APS) alumina coatings show good performance against abrasive, corrosive and erosive wear at extreme conditions of temperature, oxidation and pressure [1-3]. This is the reason why they have been widely used in applications of high exigency such as automotive, aeronautic and primary industry [4-6]. Specifically, alumina coatings are commonly used for wear resistance due to their high hardness at room temperature [7]. However, the hardness of alumina materials decreases at high temperatures as a result of micro-structural slips activated by the temperature and developed with the applied stresses [8], which is more accentuated by the presence of other oxides [9], which in turn could affect the tribological performance of alumina coatings exposed at high temperature.

Glass and cement industries use refractories subjected to extreme conditions of wear (sliding, abrasion, erosion, etc.) at high temperatures (>1000 °C), which require the employment of expensive electro-melted Al_2O_3 refractories [10]. In order to decrease the wear of the materials involved with a lower cost, different solutions have been proposed [5-6, 11-14]. Among these, thermally sprayed coatings could be an alternative solution to protect the cheap pressed & sintered refractories against tribological failures produced at high temperature. Previous studies have indicated that plasma sprayed ceramic coatings have been manufactured onto pressed & sintering refractory substrates, increasing their useful life when they are exposed to corrosive environments at high temperature and increasing the wear resistance of substrates at room temperature [5-6, 14].

The tribological performance of polycrystalline α-Al_2O_3 bulk materials has been studied indicating that until ≈ 800 ºC, the wear is produced by brittle deformation [15-17]. This last one is developed when the speed and the load applied on the material overcome its mechanical resistance, generating detachment of large and sharp particles, which acts as a third body resulting in high wear rate [18-19]. On the other hand, at higher temperatures, a plastic flux is produced in the material and then, little rounded particles are detached from the surface, producing a protective layer, which reduces the wear rate of the material and is known as ductile deformation [17-19].

The tribological performance of these materials could be related to the microstructure, the phases and their mechanical properties, and in plasma sprayed coatings, these properties are usually different to those in bulk materials due to the fast heating and quenching during the manufacturing of coatings.

The goal of this work is to evaluate the tribological behavior at different temperatures of two thermally sprayed Al_2O_3 coatings, with different structures and phase compositions, comparing the results with those obtained from both, an electro-melted Al_2O_3 bulk refractory used as reference, and a conventional pressed & sintered silico-aluminous refractory used as substrate, which were tested under the same conditions that the coatings. The first comparison is justified because the literature about wear performance of thermally sprayed Al_2O_3 coatings for temperatures as high as those used in this work is poor, and therefore, only there is available information about Al_2O_3 bulk materials. And the second comparison aims to determine the potential application of the Al_2O_3 coatings as a possible way to protect the cheap pressed & sintered refractories, to replace the expensive electro-

melted ones subjected to extreme abrasive conditions, but without structural requirements, commonly used in high exigency applications such as: glass, cement and other primary industries.

Wear tests were performed using a ball-on-disk test under dry sliding conditions from room temperature until 1000 °C, and changes in crystalline phases, porosity, micro-hardness, Young's modulus and fracture toughness experienced by the materials due to their heating during tribological tests were also evaluated.

2. MATERIALS AND METHODS

A Sulzer-Metco PTF4^{TM} plasma torch was used to spray the alumina coatings according to the parameters listed in Table 1. Two different Al_2O_3 feedstock powders were used, the first one was constituted by submicrometric agglomerated particles, and the second one was constituted by fused & crushed particles. The substrate was a commercial pressed & sintered silico-aluminous refractory brick, which was cut in shape of discs 25 mm in diameter and 7 mm in height. The arithmetic average of the surface roughness (Ra) was 12 ± 1.1 μm for the substrates, and for this reason, it was not necessary to apply a jet of abrasive particles to give them greater roughness. Therefore, only an air jet 6 bar of pressure was applied to remove particles detached from the surface.

The chemical composition and the crystallographic phases of the feedstock powders, as well as of both, the silico-aluminous refractory used as substrate and the electro-melted alumina refractory used as reference were determined using a Thermo Fisher SCIENTIFIC ARL^{TM} OPTIM'X Wavelength-Dispersive X-Ray Fluorescence (WD-XRF) spectrometer and a Bruker D8 ADVANCE X-Ray Cu Kα 1 radiation (DRX) Diffractometer respectively, using the Rietveld method for the quantification of the phases. The particle size distribution of feedstock powders was determined with a Horiba PARTICA LA-950V2 Laser Diffraction (LD) equipment. The shape of the particles, the cross sections, the surface of both coatings and the refractories, as well as the wear tracks were analyzed by Scanning Electronic Microscopy (SEM) using a JEOL JSM IT-300 LV equipment. The cross sections and surfaces of the coatings, as well as the refractories were grinded and polished according to the ASTM E1920 standard [20] in order to obtain an arithmetic average roughness (Ra) lower than 0.2 μm. The porosity was measured on the cross sections of the coatings and refractories from images taken by SEM according the indications of the ASTM E2109 standard [21] and using Image J software. Mechanical properties before and after the wear tests of all samples were determined from indentations carried out on the polished surface using a Shimadzu HMV-G 20 equipment, according with the ASTM C-1327 [22] and ASTM E-384 [23] standards. The Vickers micro-hardness, the Young's modulus and the fracture toughness from the Anstis model were calculated according to the Eq. (1-3) respectively:

$$HV = 0.0018544 \frac{P_N}{d^2} \qquad \text{Eq. (1)}$$

Where Hv is the Vickers micro-hardness [GPa], P_N is the applied normal load on the indenter [N] and d is the average length of the two diagonals produced during the indentation [mm].

$$E = \frac{-\alpha H_K}{\left(\frac{b'}{a'} - \frac{b}{a}\right)} \quad \text{Eq. (2)}$$

Where E is the Young's modulus [GPa], α is a constant ($\alpha = 0.45$), H_k is the Knoop micro-hardness [Pa], $a'$and $b'$are the longer and shorter diagonals respectively produced by the indentation [µm], and a and b are the geometric constants of the indenter ($b/a = 1/7.11$).

$$K_{IC} = 0.0016\sqrt{\frac{E}{H}}\frac{P_N}{C^{3/2}} \quad \text{Eq. (3)}$$

Where K_{IC} is the fracture toughness [MPa.m$^{1/2}$], E is the Young's modulus [GPa], H is the Vickers micro-hardness [GPa], P_N is the applied normal load on the indenter [N] and C is the longest radial crack produced during the indentation [mm].

The wear tests were performed at 25, 500, 750 and 1000 ºC with a ball-on-disk tribometer, under a dry sliding contact, without eliminating the formed debris. The wear test conditions are shown in Table 2 following some of recommendations of ASTM G-99 standard [24].

Then, the physical features of the wear tracks on the samples and the morphology of the debris produced in the wear tests were analyzed by SEM using the same equipment aforementioned, equipped with an Energy Dispersive Scanning (EDS) with an Oxford Instruments SDD X-MaxN 80 detector, which was used to determine the chemical elemental composition of these debris. Finally, the wear rate was calculated from the profile curves of wear tracks measured on the samples using a Surtronic S125 profilometer, as well the Eq. (4).

$$WR = \frac{A_s}{1000 P_N N_c} \qquad \text{Eq. (4)}$$

Where WR is the wear rate [mm^3/N.m], A_s is the wear track cross section area [µm^2], P_N is the applied normal load [N] and N_c is the total cycle number.

After tribological tests, the porosity, the crystalline phases, the micro-hardness, the Young's modulus and the fracture toughness of all samples (coatings and refractories) were evaluated again with the same equipments, standards and equations aforementioned, in order to compare the values with those obtained before the wear tests. Each measured property was determined before and after the wear tests over 3 samples, 10 times over each sample, guaranteeing statistical reproducibility and repeatability for all measurements respectively.

3. RESULTS AND DISCUSSION

The chemical composition, the particle size distribution and the crystallographic phases of the feedstock powders used to manufacture the coatings are shown in Table 3. The chemical composition results indicate that mainly Al_2O_3 constitute these materials, with particle size distributions between ≈ 21 μm and ≈ 64 μm. The main phase in the both feedstock powders was α-Al_2O_3 and additionally, in the fused & crushed one a low quantity of γ-Al_2O_3 was also detected. The morphological analysis indicated that the agglomerated powder shows rounded particles constituted by small bonded sub-micrometrical particles (Figure 1 a), evidencing that this powder was manufactured by agglomeration processes, while all particles of the fused & crushed powder were irregular with fracture marks in their surface (Figure 1 b), evidencing that this powder was manufactured by fusing and crushing processes.

On the other hand, the chemical analyses carried out to both, the silico-aluminous refractory used as substrate and the electro-melted Al_2O_3 refractory used as reference are shown in Table 4. The silico-aluminous refractory is constituted mainly by SiO_2 and Al_2O_3, while in the electro-melted one the Al_2O_3 is the predominant oxide, which is combined with SiO_2 and ZrO_2. The surface analysis of the silico-aluminous refractory suggests irregular grains with low sintering degree and therefore, low density and high porosity, 2.16 to 2.26 g/cm^3 and 16 to 20% respectively, (Figure 2 a, Table 4) typical of pressing and sintering processes of manufacturing. While the structure of the electro-melted Al_2O_3

refractory shows low porosity (less than 2%) and therefore high density (3.4 g/cm^3), (Figure 2 b, Table 4) characteristic of electro-melting processes of manufacturing.
The surface analysis of as-sprayed Al_2O_3 coatings (Figures 3 a-b) evidenced the continuous stacking of micrometrical splats typical of thermal sprayed coatings, indicating that these layers seal the pores of the silico-aluminous refractory. Additionally, on the surface coating sprayed from the agglomerated powder feedstock, sub-micrometrical particles were identified into some splats. (Figure 3 a). Furthermore, the cross-section analysis (Figures 3 c-d) allowed to establish that the thickness of both coatings was similar, 370 ± 20 µm for the coating sprayed from the agglomerated powder feedstock and 355 ± 20 µm for that made from the fused & crushed powder feedstock. Concerning the porosity (Table 5), it is possible to see that the values before and after the wear tests for all materials and all temperatures evaluated are statistically the same (all p-values are > 0.05), evidencing that there were no sintering processes.

The XRD results indicated that in both alumina coatings, α-Al_2O_3, γ-Al_2O_3 [25-28] and amorphous phase were the predominant phases (Figure 4 a-b, Table 6). In the electro-melted Al_2O_3 reference refractory used as reference, α-Al_2O_3 was the main phase (Figure 4 c, Table 6). In the uncoated silico-aluminous refractory used as substrate, mullite and silica phases were prevalent (Figure 4 d, Table 6). It is important to notice that after the spraying process for both Al_2O_3 coatings, the α-Al_2O_3 from the powder feedstock became mainly in γ-Al_2O_3 in the as-sprayed coatings. This behavior is due to the initial features of feedstock powders (Table 3) and the spraying parameters (Table 1) as it was previously mentioned by other authors [26-28]. From statistical p-values it was established that in Al_2O_3 coatings the

quantity of amorphous phase, α-Al_2O_3 and γ-Al_2O_3 has a significant change in samples tribologically tested at 1000ºC (p-values < 0.05). For its part, the mullite and silica phases percentage in the uncoated silico-aluminous refractory change significantly in the specimens tested from 750 ºC. Being of all these, more relevant the increasing of α-Al_2O_3, from the decreasing of γ-Al_2O_3 and amorphous phases produced in alumina coatings tested at 1000 ºC.

Concerning the mechanical properties (Table 7), the micro-indentation results allowed establishing that the micro-hardness of the alumina coatings manufactured from the agglomerated powder feedstock is slightly lower than that of the alumina coating manufactured from the fused & crushed powder feedstock. For both coatings, the values of micro-hardness before and after the wear tests performed at 25, 500 and 750ºC are statistically the same (p-values are > 0.05). While at 1000ºC, there are differences statistically significant (p-value are < 0.05), due to these hardness significantly increased after their heating at 1000 °C during the wear tests (Table 7), which, could be related with the increasing in the α-Al_2O_3 level produced (Table 6, Figure 4 a-b) [4, 29-30].

Particularly, for both coatings the quantities of α-Al_2O_3 detected are obtained by two ways: 1) Keeping the corundum phase of powder feedstock during thermal spraying process and 2) Promoting the formation of more corundum phase during the wear tests. The first way is explained through the presence of un-melted particles into the coating, which allow keeping the initial features of the alumina powders. Regarding the second way, the high temperature of wear tests (1000ºC), the longtime during pre-heating (≈ 2 h), the wear tests (≈ 2 h) and

the cooling (≈ 2 h) of the coatings into the furnace allow to produce the thermodynamic conditions that promote the formation of α-Al_2O_3 phase [31-32] as it is shown in Table 6 and Figure 4 a-b.

In the same way, the electro-melted Al_2O_3 refractory used as reference showed that the hardness after wear test at 1000 °C, is slightly higher than the hardness before the test (p-value < 0.05) (Table 7). This result could be attributed to the percentage decrease of m-ZrO_2 and amorphous secondary phases during the heating carried out for tribological test (Figure 4 c, Table 6). The m-ZrO_2 phase is a polymorph of ZrO_2 with low density and in general with low mechanical [33-35] and tribological properties. Regarding the silico-aluminous refractory used as substrate, although the levels of mullite phase increased and the amorphous phase decreased during wear test carried out at 1000 °C (Figure 4 d, Table 6), the hardness and fracture toughness values decreased (Table 7). This could be due to cohesive failures producing in highly porous materials due to their heating.

Some of the Young's modulus and the fracture toughness values measured before and after the wear tests carried out for all materials, presented change statistically significantly, however these may not be relevant to their tribological performance.

The tribological analysis carried out to both Al_2O_3 coatings has evidenced the development of different wear mechanisms as a function of the test temperature. In both samples evaluated at 25 ºC (Figure 5 a), were identified friction marks produced by plastic flow of the asperities in their surface due to sliding contact with the alumina ball. While in those tested at 500 °C and 750 ºC (Figure 5 b) high levels of particle detachments produced by

the propagation of cracks in the coatings, were observed, as well as fine and rounded particles which join forming small as island-shaped layers, that in some cases plug the wear tracks produced by the detachment. On the other hand, in the both coatings tested at 1000 ºC (Figure 5c) a continuous layer was formed on the wear track, consisting of fine particles, on which was observed a plastic flow.

X. Dong *et al.* [17] previously studied the change in the tribological mechanism of bulk α-Al_2O_3 as a function of temperature. They indicated that the wear was low at the beginning of the tests, with temperatures below 200 ºC and applying a normal contact stress greater than 260 MPa at 1.4 mm/s. This was due to the effect of the environmental humidity. Whereas, from this temperature and up to 800 ºC, the wear suffered by the material was severe due to the fracture of the material in the zone of contact with the counter-body. Finally, from this last temperature, the wear rate had become moderate again due to the formation of a protective layer. The normal stress applied at the beginning of the tribological tests carried out in this work was 210 MPa, however, there is a similarity in the morphological characteristics observed in the wear tracks of the samples tested at 25 °C (plastic flow), at 500 °C and 750 ºC (cracks and fractures), as well as, at 1000 ºC (formation of a protective layer), with those reported by X. Dong, *et al.* [17]. Therefore, the wear stages developed in both Al_2O_3 coatings are similar to those established by this researcher for bulk α-Al_2O_3 materials, despite the fact that the stress applied was lower. This can be related to the higher sliding speed of the ball on the coating (10 cm/s) compared to that of the bulk material (1.4 mm/s), as well as the predominant presence of the γ-Al_2O_3 phase in the coatings compared to predominant presence of the α-Al_2O_3 phase

in the bulk material. It is important to notice that the hardness of γ-Al_2O_3 is lower than that of α-Al_2O_3 [36].

G. W. Stachowiak, *et al.* [19] have studied the tribological behavior developed in ceramic materials from applied wear conditions (mainly speed and load) by the sliding contact with a counter-body also ceramic. They found that if the material was able to withstand the stress mechanically applied through the counter body, wear by ductile deformation through plastic flow in the track was produced. While in the case of the material did not have sufficient mechanical strength to withstand the stresses, the wear was produced by brittle deformation. In consequence, cracks and an excessive detachment of the particles were produced. In accordance with that established by W. Stachowiak, *et al.* [19], both types of coatings studied exhibited wear by ductile deformation when they have been tested at 25 °C and 1000 ºC. But, when they were tested at 500 °C and 750 ºC, the tribological behavior is governed by brittle deformation with higher wear rates due to excessive detachment of the particles.

Despite the fact that the sliding speed (0.1 m/s) and the applied load (5 N) were the same for all tests, a transition from ductile to brittle deformation was detected in the samples evaluated at 25 °C and 500 ºC. This result is mainly related the gradual decrease in hardness experienced by alumina as a function of the increase in temperature as previously described [8-9], promoting the detachment of particles. This behavior is more severe in the samples tested at 750 ºC, plugging the wear track. The gradual increase of the particles detachment with the temperature has favored the formation of a continuous layer which has protected the wear track of the tested samples at 1000 ºC, producing in this case, a wear

transition from brittle to ductile deformation, in which it has been again observed plastic flow (Figure 5 c). It has been previously reported that the presence of wear debris in the friction track can reduce the contact stresses on the surface of coatings, modifying the tribological conditions and therefore the wear resistance [37]. Additionally, the increase in α-Al_2O_3 detected after the wear tests carried out at 1000 ºC (Figure 4a-b, Table 4), may have had a contribution in the wear transition from fragile to ductile deformation, thanks to the fact that this phase is the hardest of the alumina materials.

Concerning the wear track of the electro-melted Al_2O_3 refractory used as reference, it was detected the same change aforementioned from ductile to fragile for returning to ductile deformation again when the temperature increased (Figure 6). A bigger quantity of debris was detected despite the fact that the tests conditions applied were the same than those for the coatings. this could be due to the low fracture toughness of this material (Table 7), increasing the wear rate compared to the coatings. For its part, the pressed & sintered silico-aluminous refractory used as substrate showed wear by brittle deformation in all cases (Figure 7). This is due to the low mechanical properties of this material shown in Table 7.

The results of wear rate calculated from the track profiles produced in each sample are shown in Table 8. For both types of coatings, their wear rate at 25 ºC was of the same order of magnitude as that measured at 1000 ºC, being lower than that determined at 500 ºC and 750 ºC, this due to the ductile-fragile-ductile transition in the tribological behavior previously explained. In addition, at the different temperatures used, the coating sprayed from the agglomerated powder showed slightly lower wear rates than those manufactured

from the fused & crushed powder, as well as, than the electro-melted refractory. This could be related to the superior resistance to crack propagation of this material and the detachment of nanometric particles from un-melted agglomerated grains, in accordance with the results of Y. An, *et al*. [38].

Regarding to the electro-melted refractory, although it has a hardness especially higher than that of the alumina coatings, its wear resistance has been lower. This result could be related, on the one hand to the excessive presence of abrasive debris between the surface and the counter-body. These debris have been analyzed by SEM-EDS, evidencing that they are angular and are composed of Al, Si, Zr and O elements from Al_2O_3, the SiO_2 and ZrO_2 phases which constitute the refractory, obtaining as a result, a third abrasive body into the system. On the other hand, the presence of SiO_2 and m-ZrO_2 can significantly reduce the high-temperature hardness of alumina-based materials [9, 33-35].

About the pressed & sintered refractory, it showed higher wear rates than all other materials evaluated, which is basically due to the poor mechanical properties of this material.
In addition, the values of friction coefficient (Table 8) measured during the high temperature tribological tests show a downward trend with respect to the temperature for all samples, which could be related to the detachment of fine particles, resulting in the formation of layers that can be protective at high temperatures. It is important to mention that the values obtained from the coefficient of friction are classic compared to the literature, between 0.7 and 0.9 for the alumina against alumina test [19].

4. CONCLUSIONS

- In this work, the tribological behavior at high temperature was evaluated for two different structures and phase compositions of Al_2O_3 coatings manufactured by APS onto a pressed and sintered silico-aluminous refractory used as substrate. The results were compared with those from an electro-melted alumina refractory used as reference and they were correlated with the phase compositions, porosities and mechanical properties measured before and after the wear tests. The tests were performed using a ball-on-disk test under dry sliding conditions from room temperature until 1000 °C.

- From the results and discussion, it was possible to conclude that the tribological behavior of both plasma sprayed Al_2O_3 coatings was governed by transitions ductile-fragile-ductile similar to those showed by the electro-melted refractory used as reference and those reported by X. Dong, *et al.* [17] for Al_2O_3 bulk materials.

- The Al_2O_3 coatings improved the wear performance of the conventional pressed & sintered silico-aluminous refractory used as substrate, even achieving the wear performance at high temperatures of the electro-melted Al_2O_3 bulk refractory used as reference, despite le fact that the Al_2O_3 coatings were mainly constituted by γ-Al_2O_3, while the electro-melted refractory was mainly constituted by α-Al_2O_3, which indicates that the higher fracture toughness in the coatings contribute to their good wear resistance.

- The possible replacement of electro-melted refractories by coated pressed and sintered refractories commonly used in glass and cement industries is only recommended in places subjected to extreme abrasive conditions, but without structural requirements like the combustion ports and the entries of raw materials.

5. ACKNOWLEDGEMENTS

- The authors are grateful to Departamento Administrativo de Ciencia, Tecnología e Innovación – Colciencias – (Bogotá – Colombia). Convocatoria Doctorado Nacional – 647 de 2014 for the Doctoral Fellowship awarded to David Franco and the CODI-Committee of the University of Antioquia for its economic support given to GIPIMME Laboratory in 2018.

6. REFERENCES

1. J. Rong, K. Yang, Y. Zhuang, H. Zhao, C. Liu, S. Tao, C. Ding, Comparative tribological study of plasma sprayed alumina and alumina-yttria under severe conditions, Surface & Coatings Technology 316 (2017) 1 – 9

2. P.A. Manojkumar, A.S. Gandhi, M. Kamaraj, A.K. Tyagi, Sliding wear behaviour of alumina coatings prepared from mechanically milled powders, Wear 313 (2014) 11 – 18

3. K. Yang, J. Rong, C. Liu, H. Zhao, S. Tao, C. Ding, Study on erosion–wear behavior and mechanism of plasma-sprayed alumina-based coatings by a novel slurry injection method, Tribology International 93 (2016) 29 – 35

4. O. Tingaud, P. Bertrand, G. Bertrand, Microstructure and tribological behavior of suspension plasma sprayed Al_2O_3 and Al_2O_3–YSZ composite coatings Microstructure and tribological behavior of suspension plasma sprayed Al_2O_3 and Al_2O_3–YSZ composite coatings, Surface & Coatings Technology 205 (2010) 1004 – 1008

5. G. Bolelli, V. Cannillo, L. Lugli, L. Lusvarghi, T. Manfredini, Plasma-sprayed graded ceramic coatings on refractory materials for improved chemical resistance, Journal of the European Ceramic Society 26 (2005) 2561 – 2579.

6. C. Bartuli, L. Lusvarghi, T. Manfredini, T. Valente, Thermal spraying to coat traditional ceramic substrates: Case studies, Journal of the European Ceramic Society 27 (2007) 1615 – 1622

7. V. P. Singh, A. Sil, R. Jayaganthan, A study on sliding and erosive wear behaviour of atmospheric plasma sprayed conventional and nanostructured alumina coatings, Materials and Design 32 (2011) 584–591

8. E. Sánchez-González, P. Miranda, J. Meléndez-Martínez, F. Guiberteau, A. Pajares, Temperature dependence of mechanical properties of alumina up to the onset of creep, Journal of the European Ceramic Society 27 (2007) 3345 – 3349

9. C. P. Alpert, H. M. Chan, S. J. Bennison, B. Lawn, Temperature Dependence of Hardness of Alumina-Based Ceramics, J. Am. Cerum. Soc. 71 [8] (1988) C-371-C-373

10. A. M. Guzmán, D.I. Martínez, R. González, Corrosion–erosion wear of refractory bricks in glass furnaces, Engineering Failure Analysis 46 (2014) 188-195

11. R. M. Khattab, S. B. Hanna, M. F. Zawrah, L. G. Girgis, Alumina–Zircon refractory materials for lining of the basin of glass furnaces: Effect of processing technique and TiO_2 addition, Ceramics International 41 [1] (2015) 1623 – 1629

12. Y. Liang, A. Huang, X. Zhu, H. Gu, L. Fu, Dynamic slag/refractory interaction of lightweight Al_2O_3–MgO castable for refining ladle, Ceramics International 41 [6] (2015) 8149 – 8154

13. G. Seifert, V. Schmitt, F. Raether, New Techniques for the Determination of Refractory Material Properties at High Temperatures, Refractories worldforum 7 [3] (2015) 77 – 84

14. G. Bolelli, V. Cannillo, L. Lusvarghi, T. Manfredini, C. Siligardi, C. Bartuli, A. Loreto, T, Valente. Plasma-sprayed glass-ceramic coatings on ceramic tiles: microstructure, chemical resistance and mechanical properties, Journal of the European Ceramic Society 25 (2005) 1835 – 1853

15. M. Woydt, K. H. Habig, High temperature tribology of ceramics, Tribology International 22 [2] (1989) 75 – 88

16. C. S. Yust, F. J. Carignan, Observations on the sliding wear of ceramics, ASLE Transactions 28 [2] (1985) 245 – 253

17. X. Dong, S. Jahanmir, S. M. Hsu, Tribological characteristics of α-alumina at elevated temperatures, J Am Ceram Soc. 74 [5] (1991) 1036 – 1044

18. K. Holmberg and A. Matthews, Tribology of engineered surfaces, in Wear - Materials, mechanisms and practice, ed. by G. Stachowiak, pub. By John Wiley & Sons, Ltd. England. 2006, Chap 7, pp. 123 – 166

19. G. W. Stachowiak and A. W. Batchelor, Wear of non-metallic materials, in Engineering Tribology (chap 16), Fourth edition, ed. by G. W. Stachowiak and A. W. Batchelor, 2013, pp. 679 – 683

20. ASTM E1920. Standard Guide for Metallographic Preparation of Thermal Sprayed Coatings, 2014

21. ASTM E2109. Standard Test Methods for Determining Area Percentage Porosity in Thermal Sprayed Coatings, 2014

22. ASTM C-1327. Standard Test Method for Vickers Indentation Hardness of Advanced Ceramics, 2008

23. ASTM E-384. Standard Test Method for Microindentation Hardness of Materials, 2017

24. ASTM G99. Standard Test Method for Wear Testing with a Pin-on-Disk Apparatus, 2017

25. J. W. Murray, A. S. M. Ang, Z. Pala, E. C. Shaw, T. Hussain, Suspension High Velocity Oxy-Fuel (SHVOF) - Sprayed Alumina Coatings: Microstructure, Nanoindentation and Wear, Journal of Thermal Spray Technology 25 [8] (2016) 1700 – 1710

26. G. Di Girolamo, A. Brentari, C. Blasi, E. Serra, Microstructure and mechanical properties of plasma sprayed alumina-based coatings, Ceramics International 40 (2014) 12861 – 12867

27. T. Tesar, R. Musalek, J. Medricky, J. Kotlan, F. Lukac, Z. Pala, P. Ctibor, T. Chraska, S. Houdkova, V. Rimal, N. Curry, Development of suspension plasma sprayed alumina coatings with high enthalpy plasma torch, Surface & Coatings Technology 325 (2017) 277 – 288

28. K. Sabiruddin, J. Joardar, P.P. Bandyopadhyay, Analysis of phase transformation in plasma sprayed alumina coatings using Rietveld refinement, Surface & Coatings Technology 204 [20] (2010) 3248 – 3253

29. V. P. Singh, A. Sil, R. Jayaganthan, A study on sliding and erosive wear behaviour of atmospheric plasma sprayed conventional and nanostructured alumina coatings, Materials and Design 32 (2011) 584 – 591

30. G. N. Heintze, S. Uematsu, Preparation and structures of plasma-sprayed γ- and α-$A1_2O_3$ coatings, Surface and Coatings Technology 50 (1992) 213 – 222

31. P. Chráska, J. Dubsky, K. Neufuss, J. Písacka, Alumina-base plasma-sprayed materials part I: Phase stability of alumina and alumina-chromia, Journal of Thermal Spray Technology 6 [3] (1997) 320 – 326

32. P. Souza Santos, H. Souza Santos, S.P. Toledo, Standard Transition Aluminas. Electron Microscopy Studies, Materials Research 3 [4] (2000) 104 – 114

33. Y. J. He, A.J.A. Winnubst, D.J. Schipper, A.J. Burggraaf, H, Verweij, Effects of a second phase on the tribological properties of $A1_2O_2$ and ZrO_2 ceramics, Wear 210 (1997) 178 – 187

34. Z. Liang, W. Wang, M. Zhang, F. Wu, J. Chen, C. Xue, H. Zhao, Structural, mechanical and thermodynamic properties of ZrO_2 polymorphs by first-principles calculation, Physica B 511 (2017) 10 –19

35. Y. Zhang, J. Zhang, First principles study of structural and thermodynamic properties of zirconia, Materials Today: Proceedings 1 (2014) 44 – 54

36. S. T. Aruna, N. Balaji, J. Shedthi, V. K. William Grips, Effect of critical plasma spray parameters on the microstructure, microhardness and wear and corrosion resistance of plasma sprayed alumina coatings, Surface & Coatings Technology 208 (2012) 92–100

37. T. E. Fischer, Z. Zhu, H. Kim, D. S. Shin, Genesis and role of wear debris in sliding wear of ceramics, Wear 245 (2000) 53 – 60

38. Y. An, S. Li, G. Hou, X. Zhao, H. Zhou, J. Chen, Mechanical and tribological properties of nano/micro composite alumina coatings fabricated by atmospheric plasma spraying, Ceramics International 43 (2017) 5319 – 5328

TABLES

Table 1. Plasma spraying parameters.

Parameter	**Agglomerated Œrlikon – Metco 6103™**	**Fused & crushed Œrlikon – Metco 6062™**
Current intensity [A]	400	650
Ar-H_2 flow rate [L/min]	45-15	
Nozzle internal diameter [mm]	7	
Feeder type	Screw Praxair	
Powder flow rate [g/min]	18	
Ar carrier gas pressure [bar]	5.0	
Ar carrier gas flow rate [L/min]	4.5	
Spray distance [mm]	100	
Sample translation speed [mm/s]	24	
Sample rotation speed [rpm]	124	
Surface substrate roughness (Ra) [µm]	8 - 10	
Cooling air distance [mm]	12	
Surface substrate preheating temperature [°C]	300	
Surface substrate preheating passes	18	12
Projection time [min]	4	
Number of spraying passes	98	96

Table 2. Wear test conditions.

Counter-body material	Alumina
Counter-body hardness [GPa]	18.0 ± 0.5
Counter-body diameter [mm]	6
Normal load [N]	5
Linear speed of the sample [m/s]	0.1
Rotation speed of the sample [rpm]	18,8
Total number of cycles	20 000
Total distance of tests [m]	628
Temperature of tests [°C]	25, 500, 750 and 1000

Table 3. Main physical-chemical features of the feedstock powders.

Properties		**Agglomerated Œrlikon – Metco 6103™**	**Fused & crushed Œrlikon – Metco 6062™**
Chemical composition [wt%]	Al_2O_3	99.9 ± 0.3	97.6 ± 0.3
	SiO_2	----------	1.0 ± 0.1
	Na_2O	----------	0.3 ± 0.0
	CaO	----------	0.3 ± 0.0
	Others	Balance	Balance
Particle size distribution [µm]	d_{10}	21.1	25.5
	d_{50}	33.3	36.8
	d_{90}	63.6	54.2
Phase analysis [wt%]	α-Al_2O_3	100.0 ± 2.8	98.8 ± 1.8
	γ-Al_2O_3	----------	1.2 ± 0.2

Table 4. Main physical-chemical features of the refractories used as substrate and as reference.

Properties		**Silico-aluminous refractory substrate Erecos ER-40™**	**Electro-melted alumina refractory RHI AG Monofrax M™**
Chemical composition [wt%]	SiO_2	52.0 ± 0.1	5.9 ± 0.1
	Al_2O_3	43.5 ± 0.2	83.8 ± 0.2
	ZrO_2	----------	5.1 ± 0.1
	Others	Balance	Balance
Phase composition [wt%]	α-Al_2O_3	2.3 ± 0.2	92.2 ± 8.3
	m-ZrO_2	----------	5.3 ± 0.8
	c-ZrO_2	----------	0.5 ± 0.1
	Cristobalite	17.9 ± 0.8	----------
	Mullite	45.4 ± 2.4	----------
	Sillimanite	20.8 ± 1.5	----------
	Amorphous	13.6 ± 3.9	2.0 ± 0.5
Apparent porosity [%]		16 - 20	≤2
Apparent density [g/cm^3]		2.16 - 2.26	3.40

Table 5. Porosity measured before and after the wear tests for all materials evaluated.

Material	Wear tests temperature [°C]	Porosity before wear tests [%]	Porosity after wear tests [%]	ANOVA p-value
Al_2O_3 coating from the agglomerated powder	25	5.4 ± 0.8	5.4 ± 0.8	1.000
	500		5.4 ± 0.7	1.000
	750		5.3 ± 0.9	0.796
	1000		5.3 ± 0.7	0.770
Al_2O_3 coating from the fused & crushed powder	25	4.5 ± 0.7	4.5 ± 0.7	1.000
	500		4.5 ± 0.4	1.000
	750		4.4 ± 0.5	0.718
	1000		4.4 ± 0.6	0.736
Electro-melted Al_2O_3 refractory used as reference	25	0.55 ± 0.08	0.58 ± 0.05	0.331
	500		0.57 ± 0.05	0.513
	750		0.52 ± 0.08	0.413
	1000		0.56 ± 0.05	0.742
Pressed & sintered silico-aluminous refractory used as substrate	25	11.50 ± 1.30	11.2 ± 1.1	0.585
	500		11.3 ± 0.7	0.675
	750		11.1 ± 0.9	0.435
	1000		11.0 ± 1.3	0.401

Table 6. Crystallographic phases detected before and after the wear tests for all materials evaluated.

Material	Variable	Wear tests temperature [°C]	Before wear tests [wt %]	After wear tests [wt %]	ANOVA p-value
Al_2O_3 coating from the agglomerated powder	α-Al_2O_3	25	14.72 ± 2.41	14.81 ± 2.43	0.935
		500		14.99 ± 1.78	0.779
		750		13.84 ± 2.81	0.463
		1000		20.76 ± 3.92	0.001
	γ-Al_2O_3	25	70.19 ± 5.45	70.33 ± 5.72	0.956
		500		71.32 ± 6.71	0.685
		750		72.88 ± 7.02	0.353
		1000		68.44 ± 4.39	0.440
	Amorphous	25	15.09 ± 3.22	14.86 ± 3.82	0.886
		500		13.69 ± 4.02	0.462
		750		13.28 ± 3.25	0.228
		1000		10.80 ± 3.36	0.010
Al_2O_3 coating from the fused & crushed powder	α-Al_2O_3	25	5.55 ± 0.81	5.63 ± 0.79	0.826
		500		5.23 ± 0.58	0.325
		750		5.44 ± 0.72	0.752
		1000		15.13 ± 1.45	0.000
	γ-Al_2O_3	25	84.05 ± 6.70	84.02 ± 6.65	0.992
		500		84.02 ± 3.42	0.990
		750		83.21 ± 5.57	0.764
		1000		75.13 ± 6.98	0.000
	Amorphous	25	10.40 ± 0.79	10.35 ± 0.83	0.894
		500		10.75 ± 1.11	0.436
		750		11.35 ± 0.83	0.020
		1000		9.74 ± 0.52	0.050
Electro-melted Al_2O_3 refractory used as reference	α-Al_2O_3	25	93.23 ± 8.34	93.58 ± 6.42	0.690
		500		93.54 ± 5.98	0.692
		750		93.28 ± 8.12	0.779
		1000		94.17 ± 7.14	0.584
	m-ZrO_2	25	5.68 ± 0.83	5.29 ± 0.83	0.307
		500		5.42 ± 0.29	0.370
		750		5.55 ± 0.58	0.690
		1000		5.18 ± 0.44	0.116
	c-ZrO_2	25	0.44 ± 0.09	0.44 ± 0.03	1.000
		500		0.42 ± 0.09	0.625
		750		0.49 ± 0.05	0.147
		1000		0.45 ± 0.07	0.785
	Amorphous	25	0.65 ± 0.09	0,69 ± 0.09	0.333
		500		0,62 ± 0.08	0.442
		750		0,68 ± 0.09	0.466
		1000		0.20 ± 0.02	0.000
Pressed & sintered silico-aluminous refractory used as substrate	α-Al_2O_3	25	2.33 ± 0.21	2.30 ± 0.23	0.764
		500		2.37 ± 0.13	0.616
		750		2.33 ± 0.18	1.000
		1000		2.83 ± 0.21	0.000
	Cristobalite	25	18.05 ± 0.83	17.95 ± 0.80	0.787
		500		18.27 ± 1.26	0.651
		750		19.06 ± 1.44	0,075
		1000		19.45 ± 1.62	0.030
	Sillimanite	25	21.61 ± 1.64	20.76 ± 1.49	0.242
		500		18.48 ± 1.30	0.000
		750		18,01 ± 0,51	0.000
		1000		17.03 ± 1.67	0.000
	Mullite	25	45.37 ± 2.12	45.39 ± 2,41	0.985
		500		46.73 ± 2.84	0.243
		750		47.65 ± 2,71	0.051
		1000		48.12 ± 2.78	0.024
	Trydimite	25	----------	----------	----------
		500		0.40 ± 0.05	----------
		750		0,98 ± 0.15	----------
		1000		2.40 ± 0.75	----------
	Amorphous	25	12.64 ± 3.80	13.60 ± 3.92	0.585
		500		13.75 ± 1.18	0.398
		750		11.97 ± 2.72	0.656
		1000		10.17 ± 2.04	0.093

Table 7. Mechanical properties measured before and after the wear tests for all materials evaluated.

Material	Variable	Wear tests temperature [°C]	Before wear tests	After wear tests	ANOVA p-value
Al_2O_3 coating sprayed from the agglomerated powder	Hardness [GPa]	25	10.02 ± 0.17	10.04 ± 0.39	0.884
		500		10.08 ± 0.38	0.657
		750		10.15 ± 0.34	0.299
		1000		12.72 ± 0.35	0.000
	Young's modulus [GPa]	25	249.4 ± 9.3	245.0 ± 11.8	0.367
		500		246.0 ± 9.1	0.419
		750		253.5 ± 12.5	0.418
		1000		251.7 ± 7.4	0.549
	Toughness [MPa.m$^{1/2}$]	25	3.75 ± 0.15	3.76 ± 0.18	0.894
		500		3.78 ± 0.14	0.650
		750		3.77 ± 0.16	0.777
		1000		3.75 ± 0.19	1.000
Al_2O_3 coating from the fused & crushed powder	Hardness [GPa]	25	10.37 ± 0.13	10.38 ± 0.12	0.860
		500		10.32 ± 0.14	0.419
		750		10.40 ± 0.23	0.725
		1000		12.26 ± 0.24	0.000
	Young's Modulus [GPa]	25	274.3 ± 23.3	272.9 ± 20.1	0.887
		500		278.8 ± 21.0	0.656
		750		278.9 ± 18.7	0.633
		1000		274.4 ± 18.1	0.992
	Toughness [MPa.m$^{1/2}$]	25	3.72 ± 0.31	3.71 ± 0.33	0.945
		500		3.74 ± 0.26	0.878
		750		3.75 ± 0.23	0.809
		1000		3.47 ± 0.29	0.040
Electro-melted Al_2O_3 refractory used as reference	Hardness [GPa]	25	13.02 ± 0.32	13.18 ± 0.43	0.359
		500		13.08 ± 0.40	0.716
		750		12.98 ± 0.15	0.727
		1000		13.31 ± 0.17	0.025
	Young's Modulus [GPa]	25	214.5 ± 27.3	213.7 ± 30.6	0.952
		500		226.4 ± 26.0	0.332
		750		221.0 ± 35.1	0.650
		1000		219.3 ± 35.2	0.738
	Toughness [MPa.m$^{1/2}$]	25	2.62 ± 0.30	2.55 ± 0.40	0.664
		500		2.58 ± 0.36	0.797
		750		2.53 ± 0.35	0.545
		1000		2.53 ± 0.32	0.525
Pressed & sintered silico-aluminous refractory used as substrate	Hardness [GPa]	25	4.08 ± 0.57	4.06 ± 0.41	0.929
		500		4.04 ± 0.51	0.871
		750		4.07 ± 0.35	0.963
		1000		3.48 ± 0.32	0.012
	Young's modulus [GPa]	25	28.9 ± 3.5	25.7 ± 4.6	0.099
		500		26.1 ± 4.0	0.114
		750		25.2 ± 2.4	0.015
		1000		26.8 ± 2.9	0.162
	Toughness [MPa.m$^{1/2}$]	25	1.47 ± 0.18	1.48 ± 0.20	0.908
		500		1.37 ± 0.27	0.345
		750		1.35 ± 0.29	0.284
		1000		1.15 ± 0.26	0.006

Table 8. Wear rate and friction coefficient for all materials evaluated.

Material	Wear tests temperature [°C]	Wear rate [mm^3/N.m]	Friction coefficient	Wear mechanism
Al_2O_3 coating sprayed from the agglomerated powder	25	$2.73\times10^{-5} \pm 9.74\times10^{-6}$	0.80 ± 0.10	Ductile deformation
	500	$2.90\times10^{-4} \pm 4.48\times10^{-5}$	0.80 ± 0.05	Brittle deformation
	750	$1.03\times10^{-3} \pm 1.96\times10^{-4}$	0.80 ± 0.03	Brittle deformation
	1000	$2.32\times10^{-5} \pm 8.49\times10^{-6}$	0.75 ± 0.04	Ductile deformation
Al_2O_3 coating sprayed from the fused & crushed powder	25	$3.33\times10^{-5} \pm 7.11\times10^{-6}$	0.97 ± 0.01	Ductile deformation
	500	$6.45\times10^{-4} \pm 1.48\times10^{-4}$	0.92 ± 0.02	Brittle deformation
	750	$1.25\times10^{-3} \pm 3.18\times10^{-4}$	0.88 ± 0.02	Brittle deformation
	1000	$3.50\times10^{-5} \pm 4.37\times10^{-6}$	0.72 ± 0.03	Ductile deformation
Electro-melted Al_2O_3 refractory used as reference	25	$2.55\times10^{-4} \pm 8.30\times10^{-5}$	0.85 ± 0.05	Ductile deformation
	500	$1.75\times10^{-3} \pm 2.32\times10^{-4}$	0.83 ± 0.03	Brittle deformation
	750	$3.90\times10^{-4} \pm 5.88\times10^{-5}$	0.77 ± 0.03	Brittle deformation
	1000	$6.00\times10^{-4} \pm 2.34\times10^{-5}$	0.74 ± 0.04	Ductile deformation
Pressed & sintered silico-aluminous refractory used as substrate	25	$1.07\times10^{-2} \pm 6.61\times10^{-3}$	0.80 ± 0.10	Brittle deformation
	500	$1.59\times10^{-2} \pm 1.19\times10^{-3}$	0.84 ± 0.04	Brittle deformation
	750	$2.41\times10^{-2} \pm 9.05\times10^{-3}$	0.75 ± 0.06	Brittle deformation
	1000	$2.31\times10^{-2} \pm 9.28\times10^{-3}$	0.70 ± 0.10	Brittle deformation

LIST OF FIGURE CAPTIONS

Figure 1. Morphology of feedstock powders: a) Agglomerated and b) Fused & crushed.

Figure 2. Surface structure of: a) Pressed & sintered silico-aluminous refractory used as substrate and b) Electro-melted Al_2O_3 refractory used as reference.

Figure 3. As-sprayed structures obtained: a-b) Surface of the Al_2O_3 coatings manufactured from the agglomerated and the fused & crushed feedstock powders respectively. c-d) Cross-section of the Al_2O_3 coatings manufactured from the agglomerated and the fused & crushed feedstock powders respectively.

Figure 4. XRD patterns at 25, 500, 750 and 1000ºC of: a) Al_2O_3 coating from the agglomerated powder, b) Al_2O_3 coating from the fused & crushed powder, c) Electro-melted Al_2O_3 refractory used as reference and d) Pressed & sintered silico-aluminous refractory used as substrate.

Figure 5. Characteristics identified on the surface of polished Al_2O_3 coatings tribologically tested at: a) 25 °C, b) 500 and 750 ºC et c) 1000 ºC.

Figure 6. Characteristics identified on the surface of electromelted refractory tribologically tested at: a) 25 °C, b) 500 and 750 ºC et c) 1000 ºC.

Figure 7. Characteristics identified on the surface of pressed and sintered refractory evaluated from room temperature until 1000 ºC.

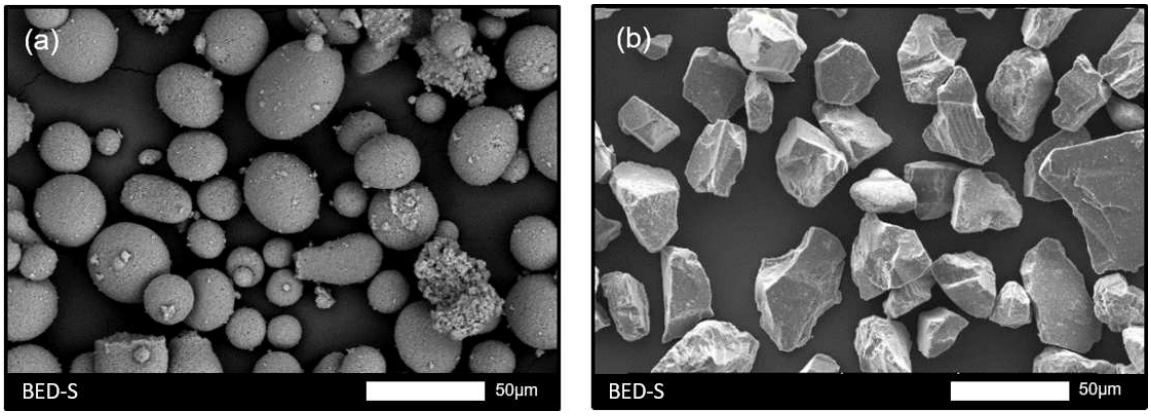


Figure 1

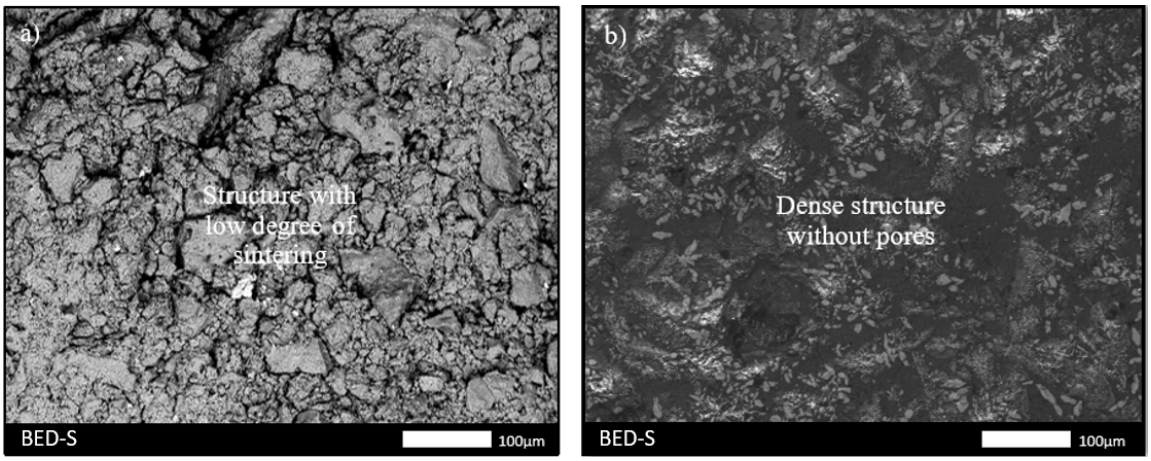

a)
Structure with
low degree of
sintering
BED-S
100µm
b)
Dense structure
without pores
BED-S
100µm

Figure 2

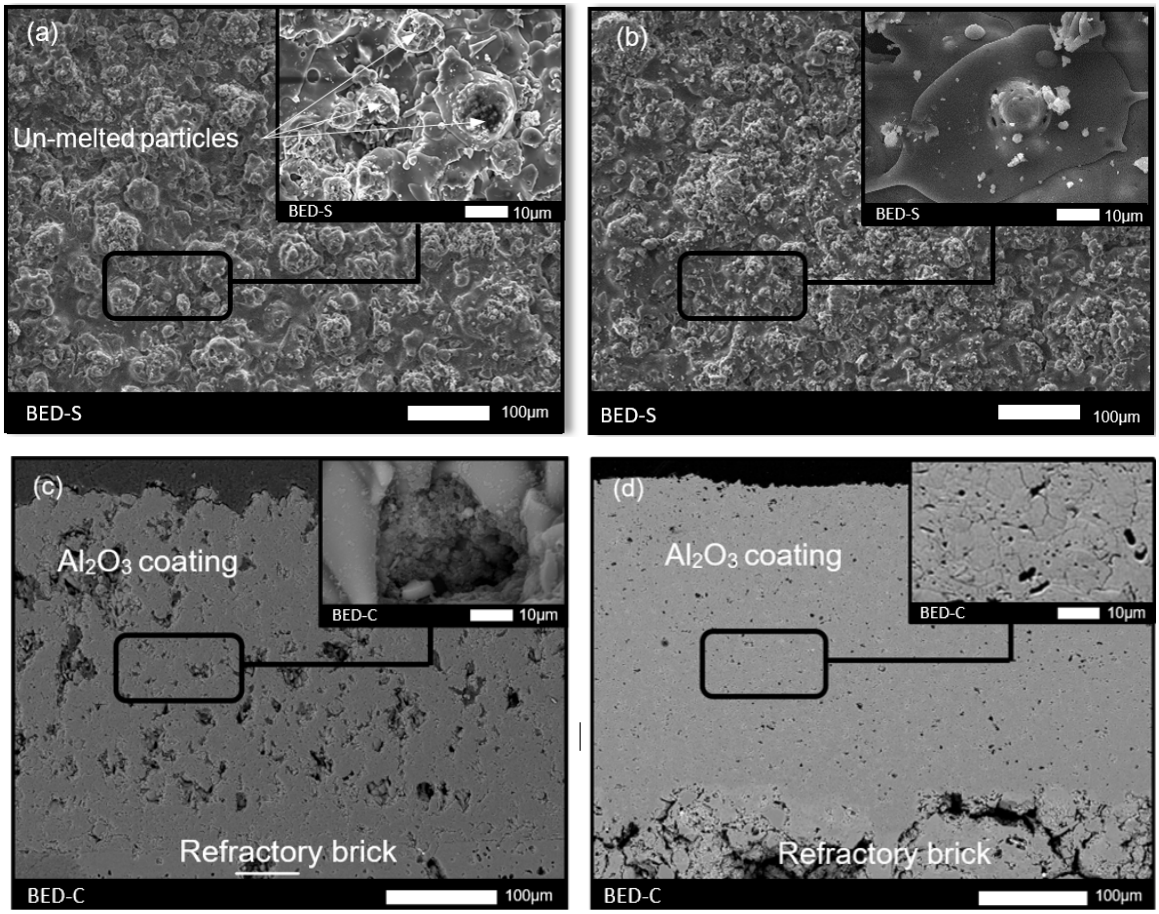
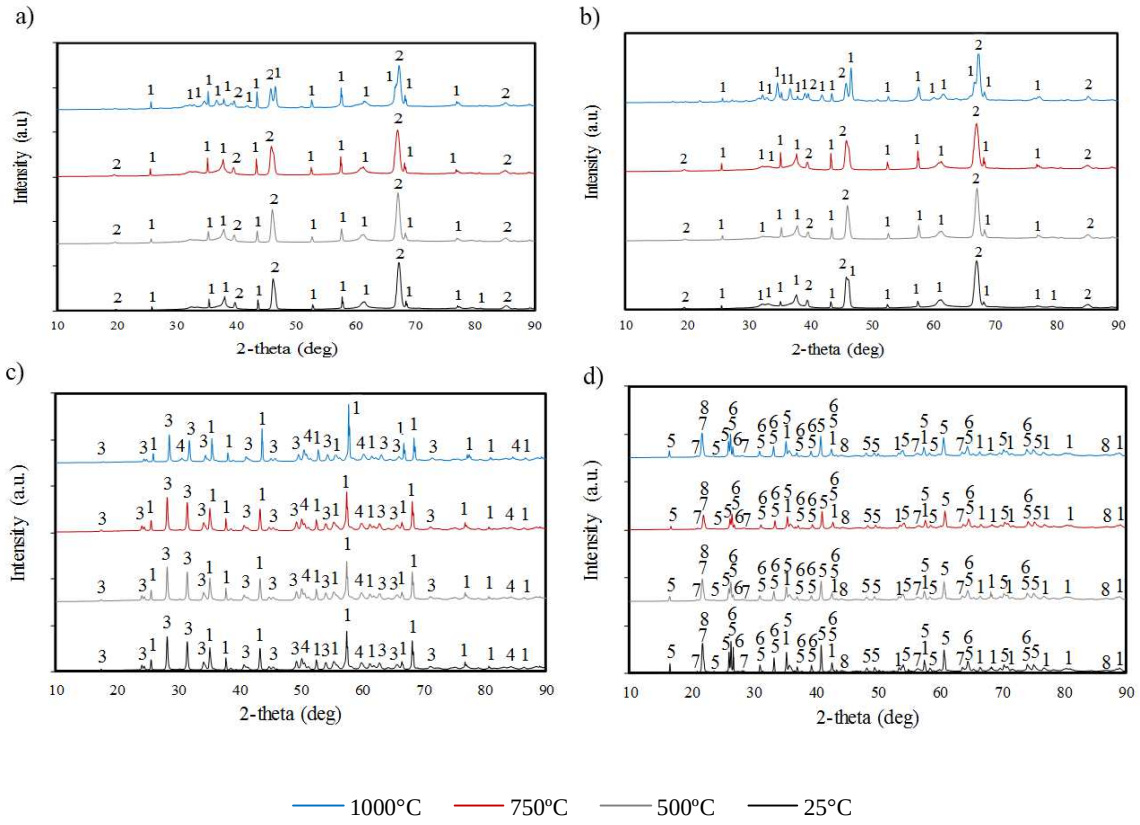

(a)
Un-melted particles
BED-S
10μm
BED-S
100μm
(b)
BED-S
10μm
BED-S
100μm
(c)
Al_2O_3 coating
BED-C
10μm
Refractory brick
BED-C
100μm
(d)
Al_2O_3 coating
BED-C
10μm
Refractory brick
BED-C
100μm

Figure 3.



1. Al_2O_3-α 2- Al_2O_3-γ 3. ZrO_2-m 4. ZrO_2-c 5. Mullite 6. Sillimanite 7. Cristobalite 8. Trydimite

Figure 4

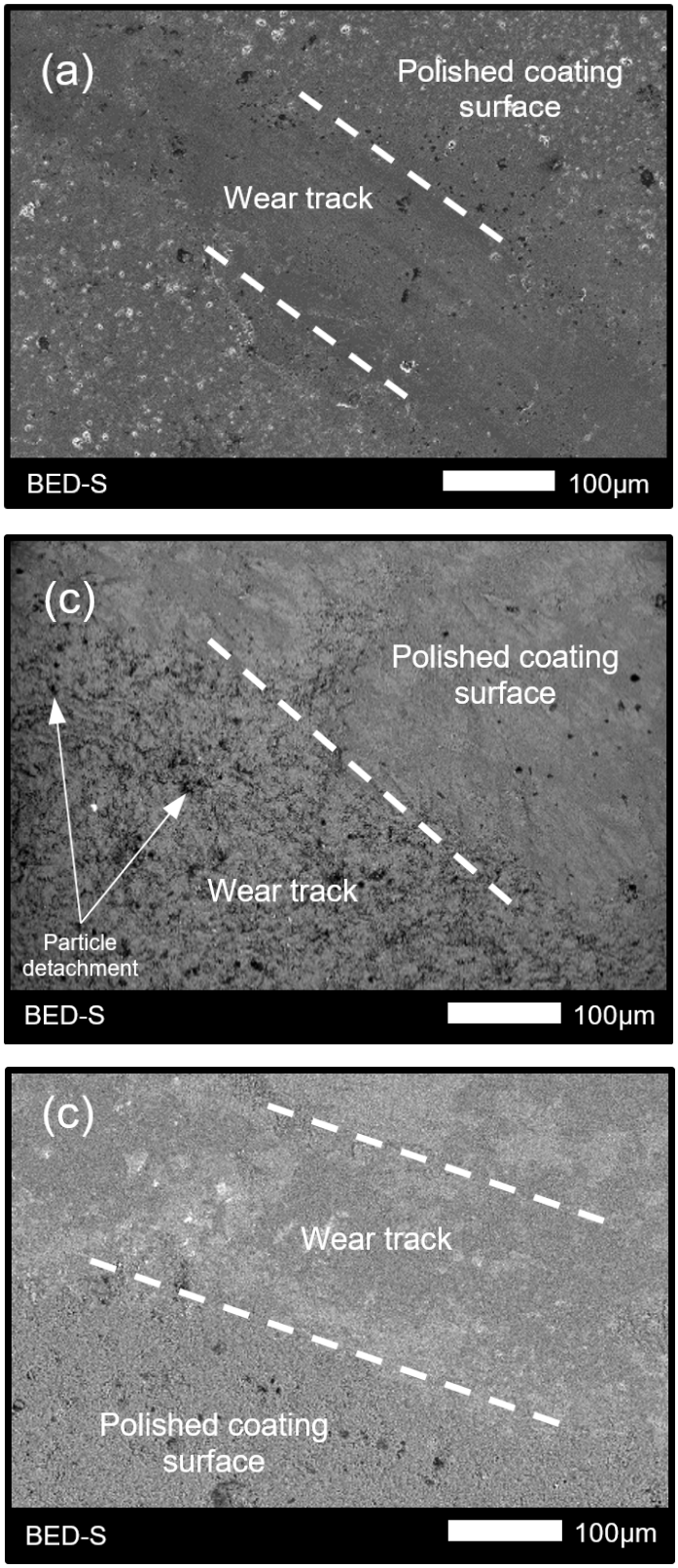
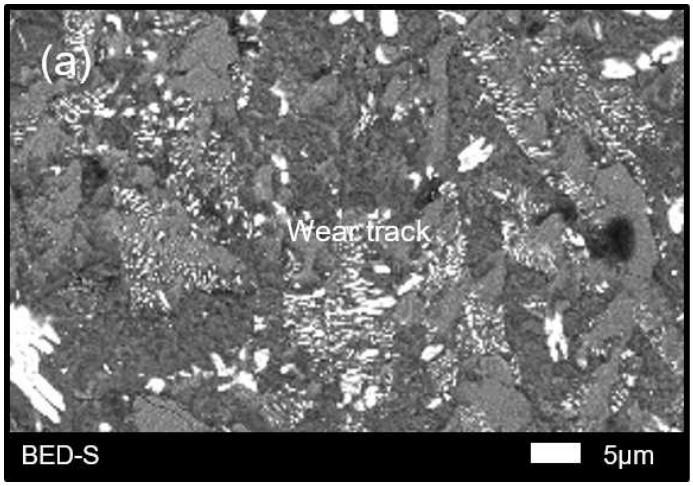
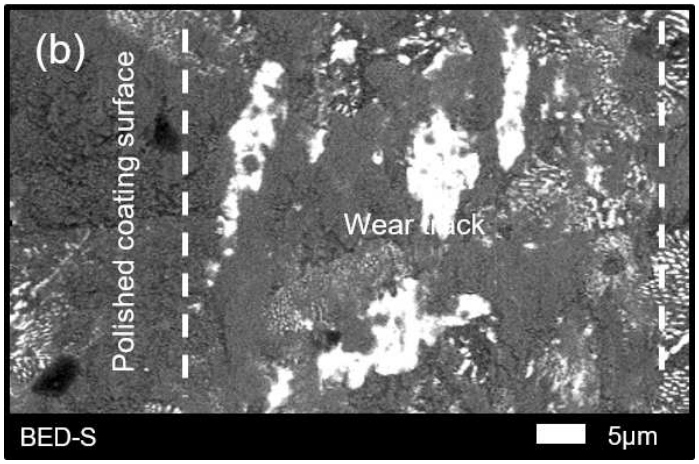

(a)
Polished coating surface
Wear track
BED-S
100µm
(c)
Polished coating surface
Wear track
Particle detachment
BED-S
100µm
(c)
Wear track
Polished coating surface
BED-S
100µm

Figure 5


(a)
Wear track
BED-S
5μm


(b)
Polished coating surface
Wear track
BED-S
5μm

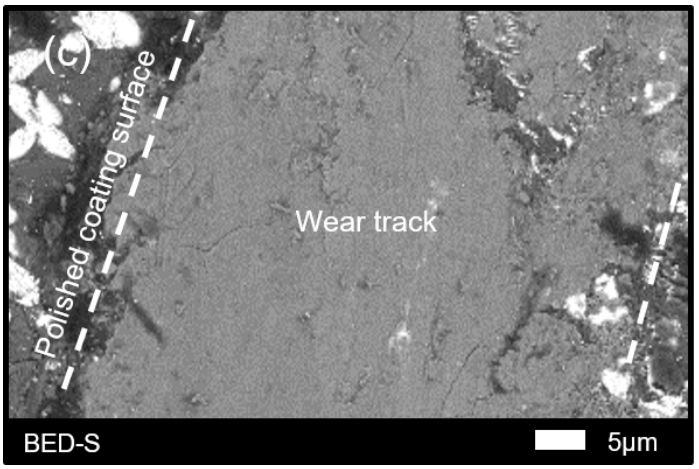

(c)
Polished coating surface
Wear track
BED-S
5μm

Figure 6

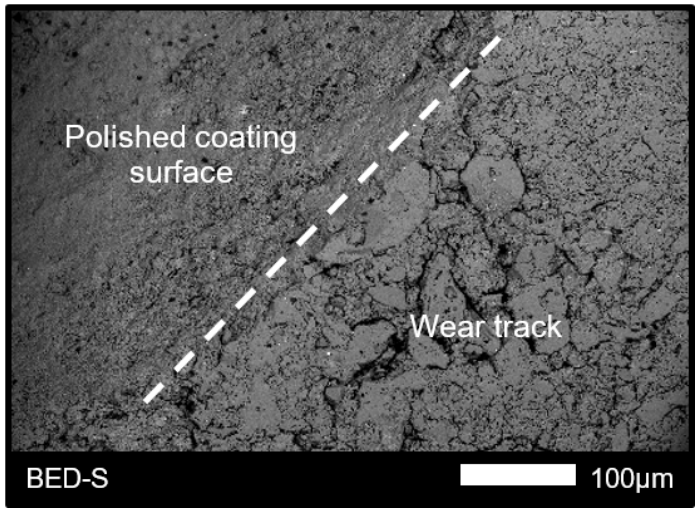


Figure 7